Microstructure and Tensile Behavior of $Al_8Co_{17}Cr_{17}Cu_8Fe_{17}Ni_{33}$ (at.%) High-Entropy Alloy

H. M. DAOUD,[1] A. MANZONI,[2] R. VÖLKL,[1] N. WANDERKA,[2] and U. GLATZEL[1,3]

1.—Metals and Alloys, University Bayreuth, Ludwig-Thoma-Str. 36b, 95447 Bayreuth, Germany. 2.—Helmholtz-Zentrum Berlin für Materialien und Energie Berlin GmbH, Hahn-Meitner-Platz 1, 14109 Berlin, Germany. 3.—e-mail: uwe.glatzel@uni-bayreuth.de

Microstructure evolution and tensile behavior of the high-entropy alloy $Al_8Co_{17}Cr_{17}Cu_8Fe_{17}Ni_{33}$ (at.%) are investigated at room temperature and at 500°C in the as-cast state and under different heat-treatment conditions. Detailed microstructural characterizations are carried out using optical microscopy, scanning electron microscopy, and transmission electron microscopy. The equilibrium phase evolution as a function of temperature was calculated using the Thermo-Calc software (Thermo-Calc Software, Stockholm, Sweden) integrated with TTNi-7 database. The observed majority phase is a face-centered cubic solid solution for all tested specimens. Tensile ductility at room temperature and at elevated temperature is enhanced by heat treatment at 1150°C. An embrittlement phenomenon has been observed after a heat treatment at 700°C resulting in significant degradation in tensile properties.

INTRODUCTION

High-entropy alloys have been developed recently and are defined as alloys containing at least five principal elements, each one having a concentration between 5 at.% and 35 at.%.[1,2] An interesting feature of the high-entropy alloys should be the formation of simple cubic solid-solution phases. Due to the high entropies of mixing in these alloys, simple solid-solution phases are expected to prevail far below the solidus temperature. Promising properties such as high corrosion and oxidation resistance, high strength, and high thermal stability are reported in the literature.[2] These properties may open the way for high-entropy alloys to be candidates for various applications at elevated temperatures, e.g., in furnace parts, molds, and tools.[2–5]

The Al-Co-Cr-Cu-Fe-Ni alloy with equal atomic contents of the elements in the as-cast state is the most widely investigated high-entropy alloy.[5–9] It has been found that increasing the Al content in the Al-Co-Cr-Cu-Fe-Ni system stabilizes the body-centered cubic (bcc) phases, which enhance the hardness and the strength of the alloy.[4,5,7] Tung et al.[5] explained this behavior by the increase of lattice distortion in the matrix due to the presence of the largest size and the strongest binding Al atoms.

Cu has a positive mixing enthalpy with all other elements, which enhances its segregation in separate phases and causes severe problems like galvanic corrosion.[10] To have a face-centered cubic (fcc) solid-solution phase, an increase of the Ni content at the expense of Al and Cu was found appropriate.[11–15]

Most available literature[4,8,16–20] highlights the compressive behavior of high-entropy alloys at room temperature where they are often found to be relatively brittle.[21] The tensile behavior is seldom reported,[20–22] and mechanical investigations at elevated temperatures are even more scarce.[4,16,21] Therefore, the tensile behavior of the selected high-entropy alloy $Al_8Co_{17}Cr_{17}Cu_8Fe_{17}Ni_{33}$ (at.%) in the as-cast state and at different heat-treated conditions both at room temperature and at 500°C is investigated in this article. The fracture mechanisms are highlighted.

EXPERIMENTAL

$Al_8Co_{17}Cr_{17}Cu_8Fe_{17}Ni_{33}$ alloy ingots were prepared from 99.99% pure elements using a vacuum-induction furnace with ingot dimensions of a cold copper mold of $100\ mm^3 \times 29\ mm^3 \times 14\ mm^3$. Three different states are investigated: as-cast and with two different heat treatments, namely one at

700°C for 5 h followed by slow cooling in air and one at 1150°C for 5 h followed by quenching in water. The microstructure of the as-cast and heat-treated specimens and fractured surfaces was characterized by optical microscopy (Zeiss Axioplan 2; Carl Zeiss, Oberkochen, Germany), scanning electron microscopy (SEM; Zeiss 1540 EsB CrossBeam workstation) equipped with an energy-dispersive x-ray (EDX) spectrometer, and transmission electron microscopy (TEM; Philips CM30 operating at 300 kV; Philips, Amsterdam, The Netherlands). The specimens for SEM observations were mechanically ground using standard metallographic procedures and finally polished with colloidal silica suspension. The specimens for TEM observations were prepared with two different methods. One of them consists in mechanical thinning down to a thickness of 10 μm and then Ar-ion milling with a voltage of 5 kV and a current of 2.5 mA in a Bal-Tec Res 101 (Leica Microsystems, Inc., Buffalo Grove, IL, USA) down to electron transparency. The other one consists in electrolytic thinning using a solution containing 83% ethanol, 10% perchloric acid, and 7% glycerin with a voltage of 20 V at −35°C. The chemical compositions of the phases were measured by TEM/EDX spectrometry with a minimum of five measurements for each phase. The grain size is obtained by the linear intercept method. The crystal structures have been obtained using an x-ray diffractometer (Bruker AXS, Billerica, MA, USA) operated with monochromatic Cu-Kα.

Room-temperature and elevated temperature tensile tests were carried out using a universal testing machine (Zwick Z100/TL35; Zwick, Kennesaw, GA, USA) at a displacement rate of 5 mm/min. Cylindrical tensile specimens with a gauge length of 25 mm and a diameter of 5 mm have been prepared according to DIN 50 125–B14x 70.[23] Heat treatments have been done in air before machining tensile specimens (the heat-treatment conditions have been mentioned previously). At room temperature, only one tensile test was carried out and two at 500°C. The equilibrium phase diagram of the investigated alloy was calculated using Thermo-Calc and the TTNi7 database.[24,25] The TTNi7 database has been developed by Thermo Tech Ltd. company (Surrey, UK) for the evaluation of the equilibrium phase diagram for Ni-based superalloys and high-Fe-containing Ni-based superalloys. The thermodynamic simulation of the TTNi database using the updated version 7 covers 21 elements, which are found in the chemical composition of various Ni-based superalloys. The simulated data provided by this database has very high accuracy in comparison with the experimental results.[24]

RESULTS

Microstructure of Al$_8$Co$_{17}$Cr$_{17}$Cu$_8$Fe$_{17}$Ni$_{33}$

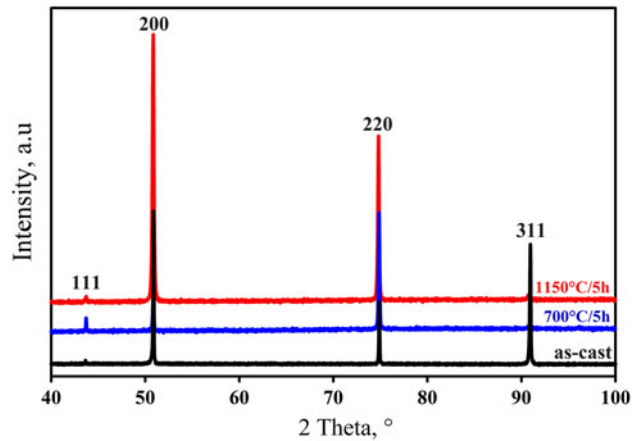Figure 1 shows the XRD patterns of the as-cast, the heat-treated at 700°C/5 h, and the heat-treated

Fig. 1. XRD patterns of as-cast and heat treated at 700°C/5 h and 1150°C/5 h specimens of the Al$_8$Co$_{17}$Cr$_{17}$Cu$_8$Fe$_{17}$Ni$_{33}$ alloy. All specimens indicate the presence of only one fcc phase. The lattice parameters are a = 357.7 pm, 357.0 pm, and 358.5 pm for the as-cast, heat-treated specimen at 700°C and at 1150°C, respectively.

at 1150°C/5 h high-entropy alloy. The XRD peaks corresponding to an fcc phase with lattice parameters a = 357.7 pm, 357.0 pm, and 358.5 pm for the as-cast, heat-treated specimens at 700°C/5 h and at 1150°C/5 h, respectively. The lattice parameters have been obtained after fitting the corresponding diffraction patterns using the Powdercell program.[26] No other phases can be singled out by XRD diffraction. However, SEM investigations indicate precipitates at the grain boundaries. Figure 2 shows SEM micrographs at low and higher magnification of all three states. Furthermore, it was found that the grain structure of all the tested specimens is columnar with an average length of 2.5 ± 0.5 mm and a width of 0.25 ± 0.1 mm, hence an aspect ratio of ~10:1.

The details of the grain boundaries at the center of the SEM images, marked by a rectangle in Fig. 2a, c, and e, are shown at higher magnification in Fig. 2b, d, and f. Small and discontinuous precipitates have been found at the grain boundaries for the as-cast alloy (see Fig. 2b). An SEM/EDX line scan analysis (not shown here) has confirmed that the precipitates are enriched in Ni, Al, and Cu. These precipitates are difficult to detect by TEM due to the discontinuity and the large grain sizes. A few Cu precipitates (volume fraction less than 1%) were also found at the grain boundaries of the as-cast alloy as reported recently.[27] The grain boundaries of the specimen heat treated at 700°C/5 h are shown in Fig. 2c and d. Two types of precipitates were found, one enriched in Ni, Al, and Cu and the other in Cr and C. The heat-treated specimen at 1150°C/5 h shown in Fig. 2e and f shows discontinuous precipitates with a low volume fraction. The chemical composition of these, however, does not indicate any particular enrichment using an SEM/EDX line scan analysis. The grain boundaries of the heat-treated at 700°C specimens have been investigated using
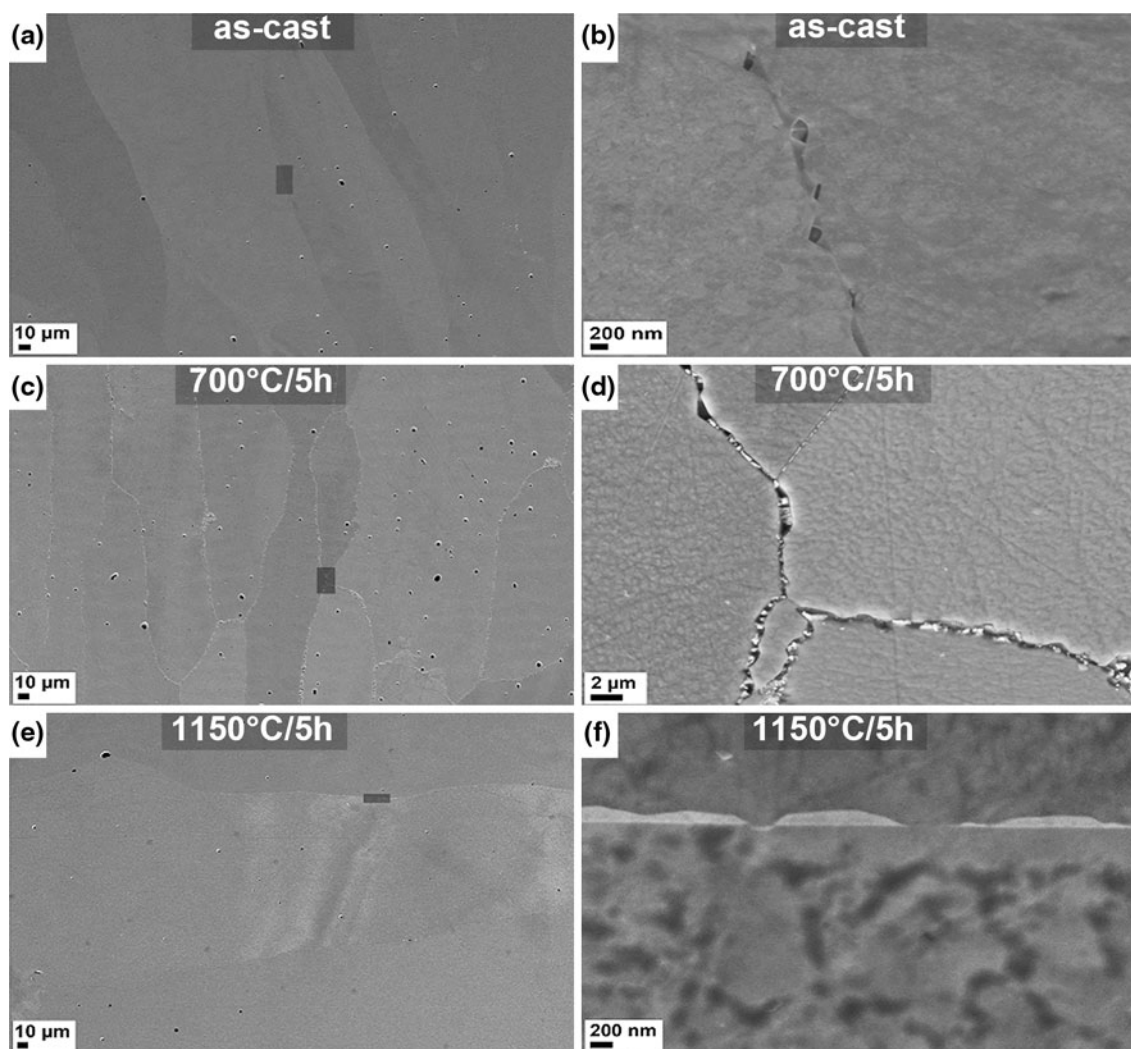
Fig. 2. SEM micrographs of the $Al_8Co_{17}Cr_{17}Cu_8Fe_{17}Ni_{33}$ alloy showing grain boundaries in: (a–b) as-cast state and after heat treatment (c–d) at 700°C/5 h and (e–f) at 1150°C/5 h. The SEM micrographs at high magnifications (b, d, f) have been taken from the marked rectangle areas located at the center of micrographs a, c, and e.

TEM in more detail and are displayed in Fig. 3. Two types of precipitates are shown in TEM micrographs in Fig. 3a and b, respectively. The corresponding diffraction patterns of each phase are shown in the inset in Fig. 3a and b. The selected-area diffraction pattern of the Cr-C-rich particle in Fig. 3a has a symmetry corresponding to a [210] zone axis pattern of an fcc phase with a lattice parameter $a = 1081$ pm. The presence of forbidden spots in the diffraction pattern of the Ni-, Al-, and Cu-rich precipitate in the [112] zone axis, shown in Fig. 3b, proves the presence of an ordered fcc phase with $L1_2$ structure, which corresponds to a γ' phase. The lattice parameter is $a = 365.2$ pm. The volume fraction of the Cr-C-rich precipitates at the grain boundaries is about three times higher than that of the γ' precipitates. SEM/EDX measurements (mappings, not shown here) indicate that the Cr-rich phase contains more carbon than surrounding areas. In addition, the diffraction pattern of Cr-rich

precipitates shows a large lattice parameter. Both factors lead to the conclusion that the phase could only be a $Cr_{23}C_6$ carbide whose structure is well known.[28]

The evolution of the microstructure inside grains with the temperature is shown in Fig. 4. Figure 4a shows the microstructure of the as-cast alloy in a dark-field image obtained using a (100) spot in the [001] zone axis. The selected area electron diffraction pattern of the [001] zone axis shows the presence of super-lattice reflections of a γ' phase with $L1_2$ structure. The size of precipitates is less than 20 nm in diameter and their volume fraction about 22%, as calculated from atom probe data.[29] This phase is enriched in Ni and Al. The microstructure of the heat-treated specimens at 700°C also reveals the presence of ~22 vol.% nanosized (~15–20 nm) γ' precipitates with $L1_2$ structure within the matrix (see Fig. 4b). Some large precipitates (length up to 350 nm) can also be observed within the grains (see
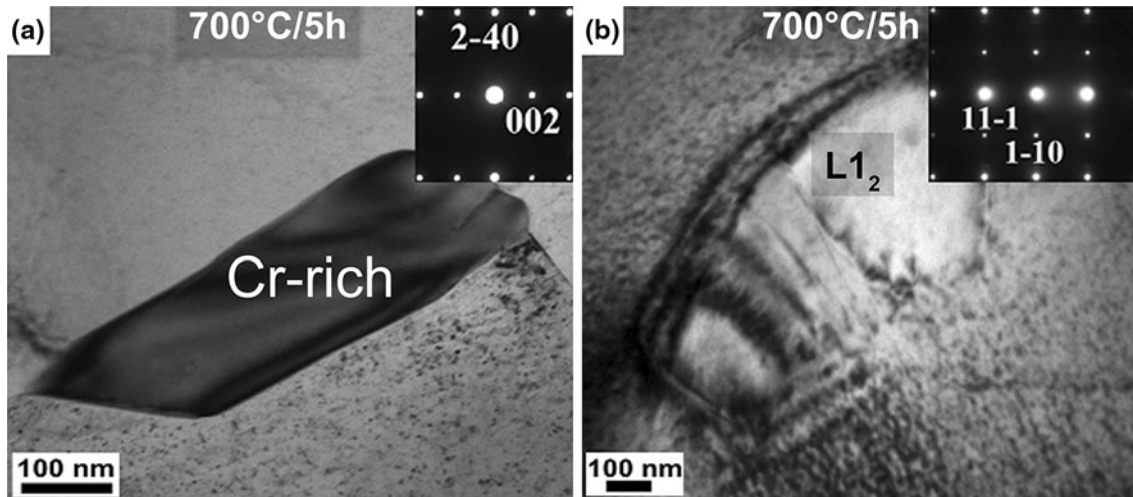
Fig. 3. Bright-field TEM images of the precipitates located at the grain boundaries of specimen heat treated at 700°C/5 h: (a) Cr-C-rich phase and the corresponding selected-area diffraction pattern along [210] zone axis in the inset and (b) Al-Ni–rich γ' phase and the corresponding selected-area diffraction pattern along [112] zone axis in the inset.

Fig. 4c). Heat treatment at 1150°C led to a decrease of the size of the γ' precipitates (<10 nm) (see Fig. 4d). Table I summarizes the microstructural features of all investigated specimens.

The chemical compositions of phases were measured by SEM/EDX and TEM/EDX and are compared with those calculated by Thermo-Calc. The simulated Thermo-Calc equilibrium phase diagram shown in Fig. 5 is simplified regarding the phases denotation when compared with that published in Ref. 27. For example the FCC-2 phase in Ref. 27 is denoted as an fcc phase in the current diagram, the "$\gamma'-1$" is now γ', the BCC-1 phase is now bcc, and the FCC-1 is fcc Cu-rich. The former phases BCC-2, FCC-3, and γ'-2 predicted by Thermo-Calc at temperatures below 500°C are not shown in Fig. 5 because they could not be observed in the current work. Information about the compositions of these unlisted phases can also be found in the Ref. 27.

Tensile Behavior

Figure 6a shows the room-temperature engineering stress–strain curves of the as-cast $Al_8Co_{17}Cr_{17}Cu_8Fe_{17}Ni_{33}$ and the alloy heat treated at 700°C/5 h and 1150°C/5 h. Yield strength, ultimate tensile strength, and uniform strain are listed in Table II.

At room temperature, the as-cast specimen shows the high strength and uniform strain (σ_{TS} = 459 MPa, ε_Y = 9%). The specimen heat treated at 1150°C/5 h exhibits extremely high uniform strain of ε_Y = 39% with the highest ultimate tensile strength (σ_{TS} = 489 MPa), whereas the specimen heat treated at 700°C exhibits brittle behavior (ε_Y = 0.1%). Figure 6b shows the stress–strain curves of $Al_8Co_{17}Cr_{17}Cu_8Fe_{17}Ni_{33}$ at 500°C. At an elevated temperature, all tested specimens exhibit lower strength than at room temperature. The ductility of the as-cast specimen decreases to

ε_Y = 0.7%. The specimen heat treated at 700°C/5 h again shows brittle behavior. However, the specimen heat treated at 1150°C behaves in a ductile way with strain to failure ε_Y = 6.0%. The as-cast and the heat-treated at 1150°C specimens show serrated stress–strain curves. The cause for the serration effects will be investigated in the near future.

Predominantly dimple structures are found in all the fractographs (Fig. 7). Extensive dimple structures are found in both the as-cast specimens (Fig. 7a) and the specimens heat treated at 1150°C/5 h (Fig. 7e), whereas almost flat fracture surfaces were observed for specimens heat treated at 700°C/5 h (Fig. 7c) and tested at room temperature. The fractographs also show that the cracks tend to propagate along interdendritic regions and grain boundaries in the fractured as-cast and heat-treated specimen at 700°C/5 h (tested at room temperature). Cracks propagate along the interdendritic regions and grain boundaries for all the tested specimens at 500°C, leading to intergranular fracture (see Fig. 7b, d, and f). An optical micrograph of an as-cast specimen (Fig. 8) highlights the crack propagation paths along the columnar grains and the interdendritic regions, as a representative micrograph for intergranular fracture.

DISCUSSION

According to Singh et al.[6] the microstructure of the as-cast equiatomic high-entropy alloy $Al_{17}Co_{17}Cr_{17}Cu_{17}Fe_{17}Ni_{17}$ consists of a Cr-Fe-rich bcc phase, an ordered bcc phase (Al-Ni-rich with B2 structure), and Cu-rich fcc phases with different morphologies. Much work was invested to simplify this structure in order to achieve better mechanical and corrosion properties.[12–14] Sheng et al.[12] reduced the Al content which eliminated the formation of the brittle bcc B2 ordered phase. The alloy
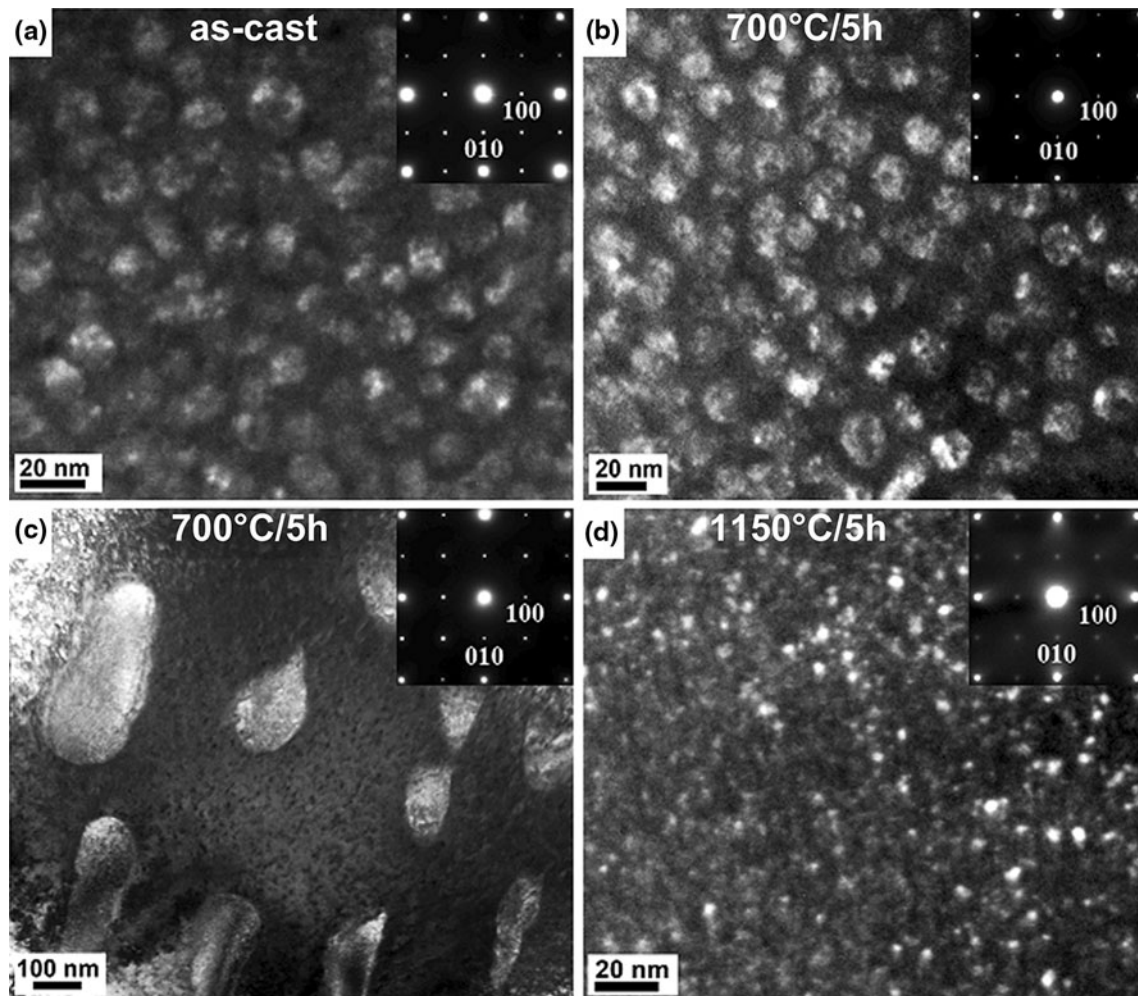
Fig. 4. Dark-field TEM images showing precipitates of a grain interior of $Al_8Co_{17}Cr_{17}Cu_8Fe_{17}Ni_{33}$ of (a) as-cast and heat-treated (b–c) at 700°C/5 h and (d) at 1150°C/5 h. The corresponding diffraction patterns of the [001] zone axis are shown in the inset, indicating ordering in the fcc phase.

Table I. Phases in the as-cast alloy and the heat treated at 700°C and at 1150°C specimens

Specimen	TEM, SEM/EDX, XRD
As-cast	Matrix: fcc solid-solution phase
	γ' precipitates (in the matrix): <20 nm, $L1_2$
	Precipitates at grain boundaries <0.7 ± 0.6%
Heat treated at 700°C/5 h	Matrix: fcc solid-solution phase
	γ' precipitates (in the matrix): spherical <20 nm and elongated <350 nm long
	γ' precipitates at grain boundaries (~250 nm–700 nm)
	Cr-rich precipitates at grain boundaries (~250 nm–500 nm)
Heat treated at 1150°C/5 h	Matrix: fcc solid-solution phase
	γ' precipitates (in the matrix): <10 nm
	Precipitates at grain boundaries <1.0 ± 0.7%

Data for as-cast specimen taken from Ref. 27.

$Al_9Co_{18}Cr_{18}Cu_{18}Fe_{18}Ni_{18}$ casted by Sheng et al.[12] showed two fcc phases: an fcc phase in the dendrite region enriched in Cr-Fe and an fcc phase in the interdendrite region enriched in Cu. Tong et al.[3] also analyzed the microstructure of the same alloy and they confirmed that in addition to the fcc
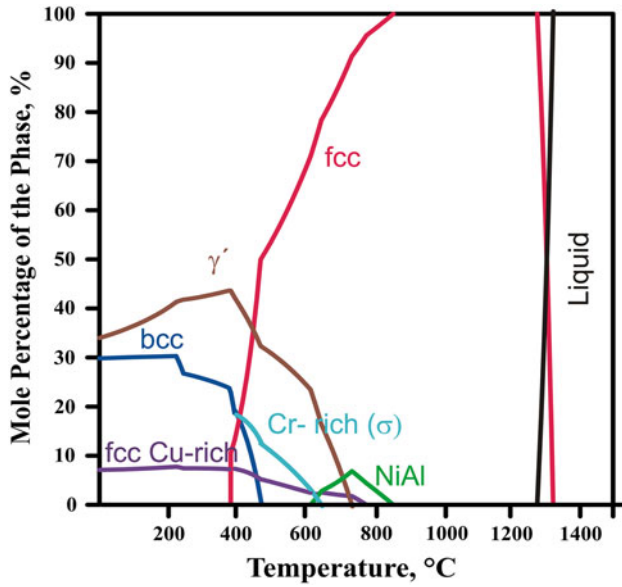
Fig. 5. Calculated phase diagram of $Al_8Co_{17}Cr_{17}Cu_8Fe_{17}Ni_{33}$, adapted from Ref. 27. Phases developing below 500°C are not shown. The compositions of the most important phases are listed in Table IV. The phase diagram was calculated using Thermo-Calc and TTNi7 database.[24,25]

Cu-rich phase in the interdendrite region and the fcc matrix phase there is an ordered fcc phase (tiny precipitates) distributed in the matrix. Furthermore, Tsai et al.[13] analyzed the microstructure of the same alloy and they reported that some bcc phases have also been found in the fcc matrix. In another work, Tsai et al.[14] have investigated an alloy with lower Al and Cu content. The microstructure of their as-cast alloy $Al_6Co_{21}Cr_{21}Cu_{10}Fe_{21}Ni_{21}$ consists of three phases. The matrix was formed by an fcc matrix phase enriched with Cr-Fe. Two different kinds of precipitates having either an fcc structure (Cu-rich) or a $L1_2$ structure were embedded in the matrix.[14]

The alloy investigated in this study had an increased Ni content in addition to reduced Al and Cu contents. Ni content has been increased to stabilize the fcc phase formation. This change simplifies the microstructure of the investigated alloy in this work because its microstructure consists mainly of an fcc solid-solution phase as the matrix and $L1_2$ nanoprecipitates. Table III summarizes and compares the microstructures of the above mentioned high-entropy alloys with the alloy investigated in this study.
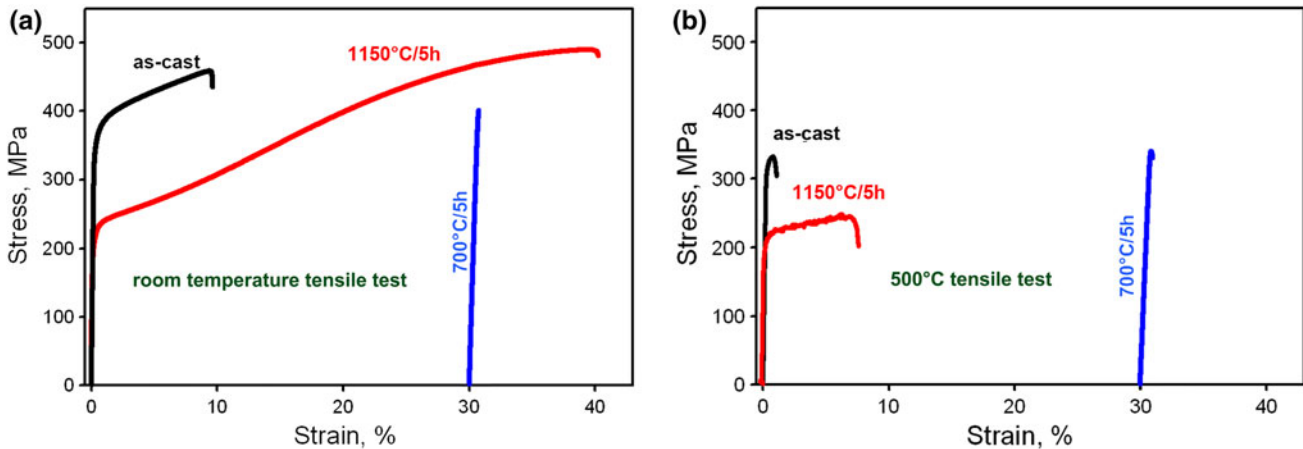

Fig. 6. Stress–strain curve of the as-cast and the heat-treated specimens at 700°C/5 h and 1150°C/5 h tested: (a) at room temperature and (b) at 500°C/5 h. In both (a) and (b), the 700°C/5 h curve is shifted to the right for better visibility.

Table II. Tensile properties of $Al_8Co_{17}Cr_{17}Cu_8Fe_{17}Ni_{33}$ (at.%) alloy

State	T (°C)	σ_Y (MPa)	σ_{TS} (MPa)	ε_{TS} (%)
As-cast	RT	357	459	9.0
Heat treated at 700°C/5 h	RT	365	365	0.1
Heat treated at 1150°C/5 h	RT	215	489	39.0
As-cast	500	315 ± 12	334 ± 1.0	0.7 ± 0.3
Heat treated at 700°C/5 h	500	310 ± 2.0	310 ± 2.0	<0.02
Heat treated at 1150°C/5 h	500	215 ± 11	248 ± 10	6.0 ± 3.0

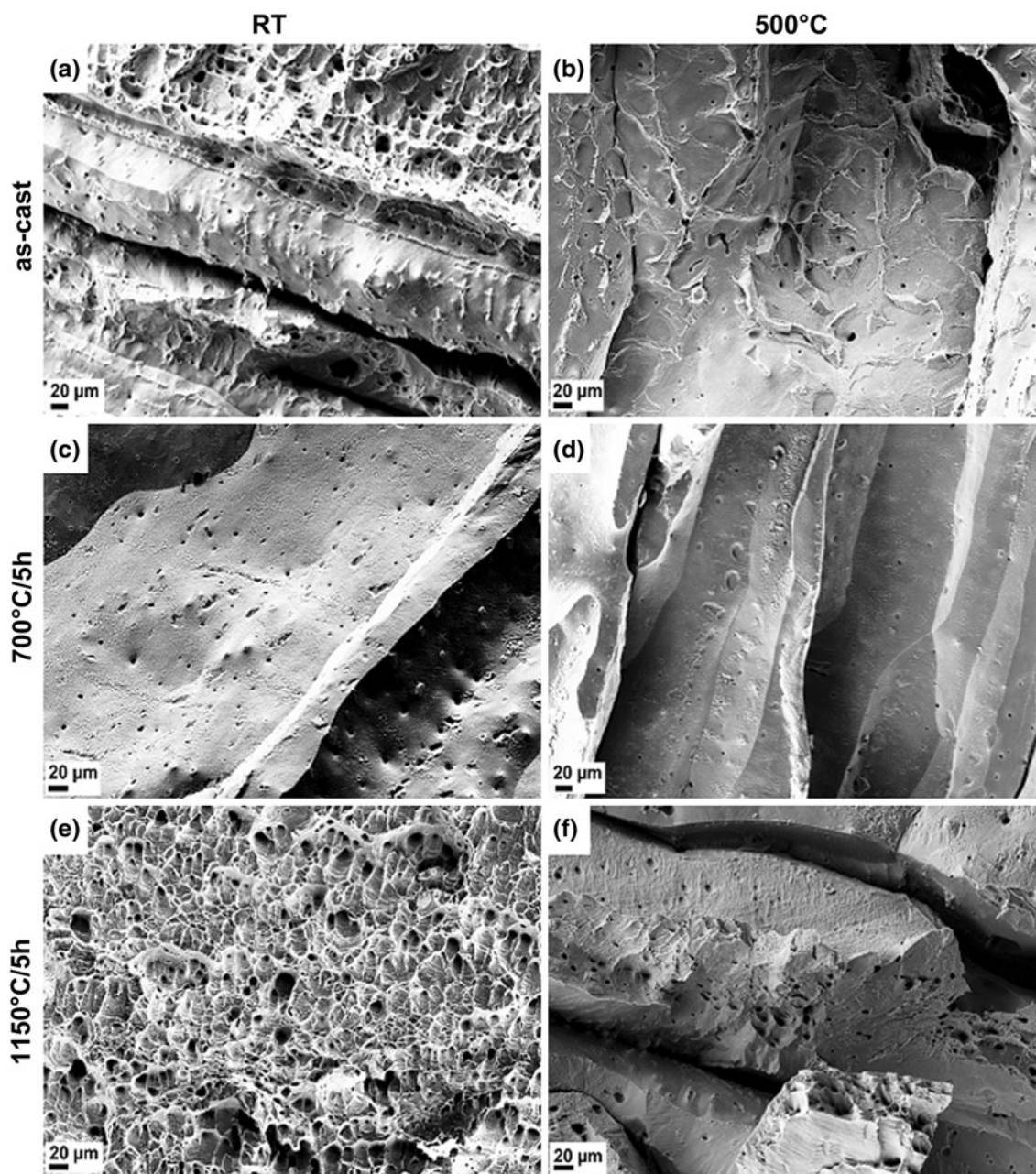The error bars correspond to the standard deviation (σ).

Fig. 7. Fractographs imaged by SEM of specimens tested at room temperature on the left side (a, c, e) and tested at 500°C/5 h on the right side (b, d, f). (a–b) as-cast; (c–d) heat treated at 700°C/5 h; (e–f) heat treated 1150°C/5 h.

According to the Thermo-Calc equilibrium phase diagram of the $Al_8Co_{17}Cr_{17}Cu_8Fe_{17}Ni_{33}$ alloy, the primary solidified phase is an fcc solid solution followed by the precipitation of a γ' and an fcc Cu-rich phase below the solidus temperature. These calculations are confirmed by the experimentally observed phases. At 700°C, in addition to these phases, a small fraction (<10%) of NiAl B2 ordered phase should be present in the temperature range of 630°C to 900°C. This phase was not observed in the current study, neither is the fcc Cu-rich phase. The predicted Cr-rich (σ) phase with the composition $Cr_{58}Fe_{33}Co_9$ is also not observed. A Cr-C phase, which has been found at the grain boundaries, corresponds to the Cr-carbide of the $M_{23}C_6$ type. This phase could not be predicted by Thermo-Calc simulations because the latter does not take into account the carbon impurities. For phases observed experimentally, the discrepancies in compositions are evident compared to those of the calculated ones (see Table IV).

At 1150°C, only an fcc solid-solution phase is expected to form. Contrary to the predication, small (<10 nm in diameter) γ' precipitates have still been observed (see Fig. 4d).

The microstructure is known to influence the mechanical properties. From the tensile tests shown

in Fig. 6, it can be observed that at room temperature both the as-cast and heat-treated specimens at 1150°C/5 h deform plastically and show a certain ductility $\varepsilon_Y = 9\%$ and $\varepsilon_Y = 39\%$, respectively. At the same temperature, the heat-treated specimen at 700°C/5 h is brittle. The ductile tensile room-temperature behavior of both the as-cast specimens and the specimens heat treated at 1150°C/5 h is due to the fact that an fcc solid solution is the main phase. FCC crystals are generally ductile because they have a large number of active slip systems and require small dislocation activation energy.[30–33] The alloy $Al_8Co_{17}Cr_{17}Cu_8Fe_{17}Ni_{33}$ heat treated at 700°C/5 h in contrast is brittle because of Cr-C-rich precipitates along the grain boundaries.

The tension strength values of all the tested specimens are low at both tested temperatures compared to, e.g., IN617 and CMSX-4 alloys at similar temperatures, despite the presence of ordered γ' precipitates (with $L1_2$ structure) in the fcc matrix. The abnormal behavior, which is often encountered in materials containing an $L1_2$ phase, could not be observed here.[34] Ordered $L1_2$ γ' phase has a great effect into increasing both the yield and
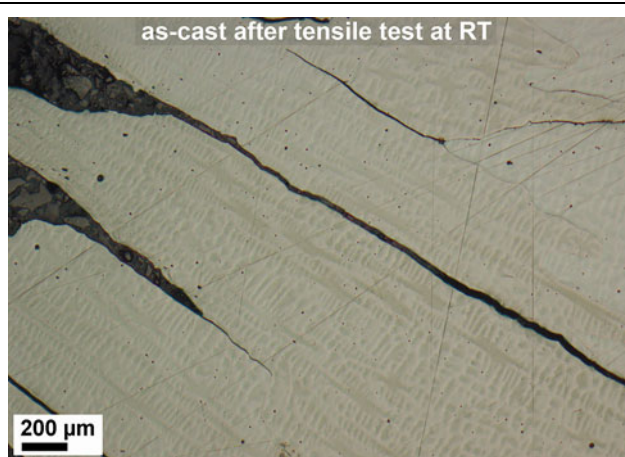

Fig. 8. Optical micrograph showing cracks propagation along the interdendritic regions or the columnar grain boundaries of $Al_8Co_{17}Cr_{17}Cu_8Fe_{17}Ni_{33}$ in the as-cast specimen tested at room temperature.

the ultimate strength with increasing temperature in several alloys, i.e., in Ni-based superalloys (e.g., single-crystal CMSX-4 Ni-based superalloy). This strengthening effect is explained by the order hardening and coherency hardening that occur due to the presence of $L1_2$ precipitates with optimum size and volume fraction in the microstructure of these alloys.[34] Beyond a certain temperature when the γ' precipitates start to dissolve, the alloy loses its strength.[34] One explanation for the low strength value measured in the current study could be due to the small size of the $L1_2$ precipitates.

The fracture mechanisms at room temperature are microvoids coalescences mixed with intergranular fracture for the as-cast and microvoids coalescences for the heat-treated specimen at 1150°C/5 h, whereas an embrittlement phenomenon (brittle fracture) is observed for the heat-treated specimen at 700°C/5 h. Even though the fcc phase is predominant, the presence of a large amount of the Cr-C-rich phase at the grain boundaries facilitates intergranular cracking, which inhibits void coalescence.[32,33]

At 500°C, both of the strength and ductility decrease for all the tested specimens. The reduced uniform strain of the as-cast specimens and the heat-treated specimens at 1150°C/5 h tested at 500°C is explained by the presence of low volume fraction of the precipitates at the grain boundaries in the microstructure of the both as-cast and heat-treated specimens at 1150°C/5 h (see Fig. 2a, b, e and f). To reveal this effect, an analysis of the microstructure of the polished fracture surfaces (< 2 mm distance to the fracture surface) of both the as-cast specimens and the heat-treated specimens at 1150°C/5 h tested at 500°C (images not shown here) has been done, and it confirms the presence of very small precipitates at the head of the propagated cracks. An SEM/EDX line scan (not shown here) has confirmed that these precipitates are rich in Ni-Al-Cu. However, the heat-treated specimen at 1150°C/5 h shows some ductility ($\varepsilon_Y = 6\%$) at 500°C. Annealing the alloy at 1150°C/5 h enhances the ductility of the specimen by making the microstructure more homogeneous and by relieving internal stresses.[31–33] In addition, a few annealing

Table III. Summary of phases obtained from the present work and from literature of similar composed high entropy alloys in the as-cast state

Alloy composition in at.%	bcc Cr-Fe rich	bcc Al-Ni rich (B2)	fcc Cr-Fe rich	fcc Cu rich (interdendrite)	fcc Cu rich (in matrix)	fcc Ni-Al-Cu rich ($L1_2$)
$Al_{17}Co_{17}Cr_{17}Cu_{17}Fe_{17}Ni_{17}$[6]	+	+	−	+	+	−
$Al_9Co_{18}Cr_{18}Cu_8Fe_{18}Ni_{18}$[3]	−	−	+	+	−	+
$Al_6Co_{21}Cr_{21}Cu_{10}Fe_{21}Ni_{21}$[14]	−	−	+	−	+	+
$Al_8Co_{17}Cr_{17}Cu_8Fe_{17}Ni_{33}$ (this work)	−	−	+	−	−	+

+ indicates present, − not present.

Table IV. Compositions (at.%) of the phases in $Al_8Co_{17}Cr_{17}Cu_8Fe_{17}Ni_{33}$ alloy heat treated at 700°C/5 h, measured by 3D-AP (Data from Paper in Preparation) and TEM-EDX, and compared with equilibrium phases predicted by thermo-calc and TTNi7 database[24,25]

Method	Denomination in the text or figures, respectively	Al	Co	Cr	Cu	Fe	Ni	C	Size (nm)	Volume fraction (%)
3D-AP	fcc-Matrix (Cr-Fe rich)	5.1 ± 0.3	19.3 ± 0.5	19.2 ± 0.2	4.0 ± 0.8	19.9 ± 0.8	32.5 ± 0.3	–	–	Balance
	γ'—in grains (Ni-Al-Cu rich, small)	22.4 ± 1.7	9.5 ± 0.9	5.5 ± 1.1	11.2 ± 1.4	6.9 ± 1.4	44.5 ± 1.6	–	~20	~22
	γ'—in grains (Ni-Al-Cu rich, large)	23.6 ± 3.1	6.7 ± 2.4	4.6 ± 1.9	14.9 ± 1.6	5.7 ± 2.4	44.6 ± 2.4	–	~250–350	<1
TEM-EDX	γ'—at grain boundaries (Ni-Al-Cu rich)	22.9 ± 2.8	5.5 ± 2.3	2.5 ± 1.4	17.1 ± 1.5	4.2 ± 1.9	47.8 ± 2.5	–	~250–700	<1
	Cr-C rich precipitates at grain boundaries	(0.6 ± 0.3)	4.0 ± 0.2	84.4 ± 1.1	0.5 ± 0.2	6.6 ± 0.5	$(3.9 \pm 0.4)_{1-x}$	x	~250–500	81
Thermo-Calc $T = 700°C$	fcc-matrix (Cr-Fe rich)	5.0	18	20	4.0	20	33	–	–	9
	γ' (Ni-Al-Cu rich)	21.3	7.7	5.1	12.8	2.1	51.0	–	–	0
	Cr rich (σ)	–	–	–	–	–	–	–	–	2
	fcc (Cu rich)	3.1	13.1	0.2	75.4	0.6	7.6	–	–	8
	B2 (Ni-Al rich)	32.8	8.6	3.4	2.1	5.6	47.5	–	–	0.5
Thermo-Calc $T = 650°C$	Cr rich (σ)	0.0	23	58	0	13	6	–	–	

The errors bars correspond to the standard deviation 2σ.

Fig. 9. Optical micrograph of $Al_8Co_{17}Cr_{17}Cu_8Fe_{17}Ni_{33}$ heat treated at 1150°C/5 h alloy showing annealing twins.

twins (see Fig. 9) are formed, an effect often observed in fcc crystals annealed at high temperatures.[30,32] These twins provide an additional possible mode of plastic deformation, thus slightly increasing ductility.[30,32,35,36] However, detailed work should be done to investigate this. Specimens that were heat treated at 700°C/5 h maintain their brittle behavior when tension tested at 500°C due to a large distribution of Cr-C-rich precipitates along the grain boundaries (see Fig. 2c and d).

Intergranular fractures with some dimples formation are the fracture mechanisms in the case of the as-cast specimen tested at 500°C. The fracture mechanism of the heat treated specimen at 700°C/5 h is intergranular fracture without void coalescence the same as at room temperature. The heat-treated specimen at 1150°C fractures in intergranular mode mixed with void-coalescence at 500°C. The detailed fracture mechanisms for high-entropy alloys demand further investigations.

CONCLUSIONS

The microstructure of the as-cast and heat treated $Al_8Co_{17}Cr_{17}Cu_8Fe_{17}Ni_{33}$ high-entropy alloy reveals an fcc solid solution as the main phase. The tensile behavior at 500°C in comparison with room temperature shows a decrease in both strength and ductility. The alloy heat treated at 700°C shows embrittlement behavior due to the presence of a Cr-C-rich phase at the grain boundaries. Annealing at 1150°C/5 h leads to maximum ductility. The fracture mechanism of the tested specimens reveals signatures of ductile failure (void coalescences) for the as-cast specimen and for the one heat treated at 1150°C/5 h. The brittle mode is evident for specimens heat treated at 700°C/5 h (at room temperature and 500°C).

ACKNOWLEDGEMENTS

REFERENCES

1. J.W. Yeh, S.K. Chen, S.J. Lin, J.Y. Gan, T.S. Chin, T.T. Shun, C.H. Tsau, and S.Y. Chang, *Adv. Eng. Mater.* 6, 299 (2004).
2. J.W. Yeh, Y.L. Chen, S.J. Lin, and S.K. Chen, *Mater. Sci. Forum* 560, 1 (2007).
3. C.J. Tong, Y.L. Chen, S.K. Chen, J.W. Yeh, T.T. Shun, C.H. Tsau, S.J. Lin, and S.Y. Chang, *Metall. Mater. Trans. A* 36, 881 (2005).
4. C.J. Tong, M.R. Chen, S.K. Chen, J.W. Yeh, T.T. Shun, S.J. Lin, and S.Y. Chang, *Metall. Mater. Trans. A* 36A, 1263 (2005).
5. C.C. Tung, J.W. Yeh, T.T. Shun, S.K. Chen, Y.S. Huang, and H.C. Chen, *Mater. Lett.* 6, 1 (2007).
6. S. Singh, N. Wanderka, B.S. Murty, U. Glatzel, and J. Banhart, *Acta Mater.* 59, 182 (2011).
7. J.M. Wu, S.J. Lin, J.W. Yeh, S.K. Chen, Y.S. Huang, and H.C. Chen, *Wear* 261, 513 (2006).
8. L.H. Wen, H.C. Kou, J.S. Li, H. Chang, X.Y. Xue, and L. Zhou, *Intermetallics* 17, 266 (2009).
9. K.B. Zhang, Z.Y. Fu, J.Y. Zhang, J. Shi, W.M. Wang, H. Wang, Y.C. Wang, and Q.J. Zhang, *J. Alloys Compd.* 502, 295 (2010).
10. Y.J. Hsu, W.C. Chiang, and J.K. Wu, *Mater. Chem. Phys.* 92, 112 (2005).
11. T.T. Shun, C.H. Hung, and C.F. Lee, *J. Alloys Compd.* 493, 105 (2010).
12. H.F. Sheng, M. Gong, and L.M. Peng, *Mater. Sci. Eng. A* 567, 14 (2013).
13. C.W. Tsai, Y.L. Chen, M.H. Tsai, J.W. Yeh, T.T. Shun, and S.K. Chen, *J. Alloys Compd.* 486, 427 (2009).
14. M.H. Tsai, H. Yuan, G. Cheng, W. Xu, K.Y. Tsai, C.W. Tsai, W.W. Jian, C.C. Juan, W.J. Shen, M.H. Chuang, J.W. Yeh, and Y.T. Zhu, *Intermetallics* 32, 329 (2013).
15. S. Guo, C. Ng, and C.T. Liu, *J. Alloys Compd.* 557, 77 (2013).
16. O.N. Senkov, G.B. Wilks, J.M. Scott, and D.B. Miracle, *Intermetallics* 19, 698 (2011).
17. K.B. Zhang, Z.Y. Zhang, W.M. Wang, H. Wang, Y.C. Wang, Q.J. Zhang, and J. Shi, *Mater. Sci. Eng. A* 508, 214 (2009).
18. F.J. Wang, Y. Zhang, and G.L. Chen, *J. Alloys Compd.* 478, 321 (2009).
19. O.N. Senkov, J.M. Scott, S.V. Senkova, D.B. Miracle, and C.F. Woodward, *J. Alloys Compd.* 509, 6043 (2011).
20. F. Wang, Y. Zhang, and G. Chen, *Inter Int. J. Mod. Phys. B* 23, 1254 (2009).
21. A.V. Kuznetsov, D.G. Shaysultnov, N.D. Stepanov, G.A. Salishchev, and O.N. Senkov, *Mater. Sci. Eng. A* 533, 107 (2012).
22. T.T. Shun and Y.C. Du, *J. Alloys Compd.* 479, 157 (2009).
23. DIN Deutsches Institut für Normung e.v. (Hrsg.), *DIN-Taschenbuch 205, Materialprüfnormen für metallische Werkstoffe 3- Mechanische-technologische Prüfverfahren (erzeugnisformabhängig), Schweißverbindungen, Metallklebungen*, 3rd ed. (Berlin, Germany: Beuth Verlag, 1996), pp. 44–51.
24. The Version TCCR, ThermoCalc Software AB, Stockholm, Sweden, 2006, http://www.thermocalc.com.
25. *Thermotech Ni-Based Superalloys Database, TTNI7, Version 7.0* (Stockholm, Sweden: Thermo-Calc Software AB, 2006).
26. Federal Institute for Materials Research and Testing, Powdercell for windows, version 2.4, 2000, http://www.ccp14.ac.uk/ccp/web-mirrors/powdcell/a_v/v_1/powder/e_cell.html.
27. A. Manzoni, H. Daoud, S. Mondal, S. van Smaalen, R. Völkl, U. Glatzel, and N. Wanderka, *J. Alloys Compd.* 552, 430 (2013).
28. A.L. Bowman, G.P. Arnold, E.K. Storms, and N.G. Nereson, *Acta Cryst.* B28, 3102 (1972).
29. D. Blavette, P. Caron, and T. Khan, *Superalloys*, ed. D.N. Duhl, G. Maurer, S. Antolovich, C. Lund, and S. Reichman (Warrendale, PA: TMS, 1988), pp. 305–314.
30. F.J. Humphreys and M. Hatherly, *Recrystallization and Related Annealing Phenomena*, 2nd ed. (Oxford: Elsevier Ltd., 2004), p. 628.
31. W.F. Smith and J. Hashemi, *Foundations of Materials Science and Engineering*, 5th ed. (New York: Mc Graw-Hill Book Co, 2011), pp. 244–268.
32. G.E. Dieter, *Mechanical Metallurgy*, ed. S.I. Metric (Singapore: Mc Graw-Hill Book Co., 1988), pp. 132–135, 233–236, 254–265.
33. J. Roesler, *Mechanical Behavior of Engineering Materials, Metals, Ceramics, Polymers and Composites* (Berlin, Germany: Springer, 2007), pp. 114–116, 173–178, 185–195.
34. A. Sengupta, S.K. Putatunda, L. Bartosiewicz, J. Hangas, P.J. Nailos, M. Peputapeck, and F.E. Alberts, *J. Mater. Eng. Perform.* 3, 664 (1994).
35. S. Ifergane, Z. Barkay, O. Beeri, and N. Eliaz, *J. Mater. Sci.* 45, 6345 (2010).
36. J.E. Flinn, D.P. Field, G.E. Korth, T.M. Lillo, and J. Macheret, *Acta Mater.* 49, 2065 (2001).